Annals of Botany **127**: 191–201, 2021
doi: 10.1093/aob/mcaa102, available online at www.academic.oup.com/aob

ANNALS OF BOTANY
Founded 1887

Inter- and intraspecific variation in grass phytolith shape and size: a geometric morphometrics perspective

Kristýna Hošková[1,*], Adéla Pokorná[1,2], Jiří Neustupa[1] and Petr Pokorný[3]

[1]Department of Botany, Faculty of Sciences, Charles University in Prague, Benátská 2, CZ-128 01 Praha 2, Czech Republic; [2]Institute of Archaeology, Czech Academy of Sciences, Letenská 4, CZ-11801 Praha 1, Czech Republic and [3]Center for Theoretical Study, Joint Research Institute of Charles University and Czech Academy of Sciences, Husova 4, CZ-110 00 Praha 1, Czech Republic
**For correspondence. E-mail kristyna.kuncova@natur.cuni.cz*

Received: 4 March 2020 Returned for revision: 8 April 2020 Editorial decision: 13 May 2020 Accepted: 22 May 2020
Electronically published: 28 May 2020

• **Background and Aims** The relative contributions of inter- and intraspecific variation to phytolith shape and size have only been investigated in a limited number of studies. However, a detailed understanding of phytolith variation patterns among populations or even within a single plant specimen is of key importance for the correct taxonomic identification of grass taxa in fossil samples and for the reconstruction of vegetation and environmental conditions in the past. In this study, we used geometric morphometric analysis for the quantification of different sources of phytolith shape and size variation.
• **Methods** We used landmark-based geometric morphometric methods for the analysis of phytolith shapes in two extant grass species (*Brachypodium pinnatum* and *B. sylvaticum*). For each species, 1200 phytoliths were analysed from 12 leaves originating from six plants growing in three populations. Phytolith shape and size data were subjected to multivariate Procrustes analysis of variance (ANOVA), multivariate regression, principal component analysis and linear discriminant analysis.
• **Key Results** Interspecific variation largely outweighed intraspecific variation with respect to phytolith shape. Individual phytolith shapes were classified with 83 % accuracy into their respective species. Conversely, variation in phytolith shapes within species but among populations, possibly related to environmental heterogeneity, was comparatively low.
• **Conclusions** Our results imply that phytolith shape relatively closely corresponds to the taxonomic identity of closely related grass species. Moreover, our methodological approach, applied here in phytolith analysis for the first time, enabled the quantification and separation of variation that is not related to species discrimination. Our findings strengthen the role of grass phytoliths in the reconstruction of past vegetation dynamics.

Key words: Phytolith analysis, intraspecific variation, landmark-based geometric morphometrics, generalized Procrustes superimposition, paleoecology, *Brachypodium pinnatum*, *Brachypodium sylvaticum*.

INTRODUCTION

The analysis of microfossil silica phytoliths is becoming an increasingly important research tool in paleoecology and archeobotany (Piperno, 2006; Hart, 2016; Strömberg *et al.*, 2018). Phytoliths are formed in plant tissues as a result of the precipitation of monosilicic acid (H_4SiO_4) taken from soil water by roots, and are thought to function either as a structural support or in alleviation of ecological stresses (e.g. defence against herbivores and pathogen resistance) (e.g. Epstein, 2009; Cooke *et al.*, 2011; Strömberg *et al.*, 2016; Katz, 2019). After being released from decaying plant material, phytoliths persist in a broad spectrum of sedimentary conditions (Piperno, 2006). Thus, due to their proven taxonomic relevance, phytoliths have been applied in various reconstructions of long-term vegetation dynamics (e.g. Delhon *et al.*, 2003; Neumann *et al.*, 2009; Barboni *et al.*, 2010; McCune *et al.*, 2015), usually represented by the vegetation type (or plant functional units) proportions (e.g. savannah/forest or grasses/woody plants ratios). A considerable number of investigations have been focused mainly on grass-dominated ecosystems (Alexandre *et al.*, 1997; Fredlund and Tieszen, 1997; Blinnikov *et al.*, 2002; Strömberg *et al.*, 2007; Evett and Bartolome, 2013; Evett and Cuthrell, 2013), since grasses are particularly silica rich with diagnostic phytolith shapes (Prychid *et al.*, 2003; Schoelynck *et al.*, 2010; Katz, 2015). Surprisingly, only little is known about the relative importance of various factors influencing the observed variation in grass phytolith shape and size (Ball and Brotherson, 1992; Whang *et al.*, 1998; Out and Madella, 2016, 2017; Zhang *et al.*, 2018).

There are, apparently, multiple sources of phytolith shape and size variation in grasses. One is the result of phylogeny. Numerous studies have demonstrated varying phytolith morphology among taxa at the level of different subfamilies, tribes, genera or, in a few cases, even individual species (e.g. Metcalfe, 1960; Twiss *et al.*, 1969; Renvoize, 1987; Mulholland and Rapp, 1992; Lu and Liu, 2003; Fahmy, 2008; Out and Madella, 2016). The close relationship between phytolith shape and the phylogenetic position of a species applies particularly to grass silica

short cell (GSSC) phytoliths, where silica deposition occurs as a result of a genetically determined active process taking place in viable cells (e.g. Hodson *et al.*, 2005; Kumar *et al.*, 2017). Furthermore, grass inflorescence phytoliths can be used as an effective tool for discriminating between species (Rosen, 1992; Ball *et al.*, 1999; Portillo *et al.*, 2006; Ge *et al.*, 2018; Zhang *et al.*, 2018). Environmental conditions have also been reported as another possible source of variation in both phytolith size and their concentration in plant tissues (Tsartsidou *et al.*, 2007; Madella *et al.*, 2009; Katz *et al.*, 2013; Liu *et al.*, 2016) (the implications of this for the application of phytolith analysis in archaeology, etc., were also discussed in Shillito *et al.*, 2013), but several studies have argued for the dominant role of phylogenetic distance in determining phytolith shape variation (Ball and Brotherson, 1992; Out and Madella, 2016). However, for the precise taxonomic identification of grasses, and thus for the reconstruction of past vegetation and environmental conditions in more detail, an understanding of how the grass phytolith shape and size vary among populations or even within a single specimen is of key importance.

Intraspecific variation in phytolith shape and size has several sources on different scales. For example, variation between populations of the same species may have resulted from different environmental conditions experienced by individual plants, but could also have been influenced by differences between genotypes. Previous studies have not only shown that various phytoliths occur in different plant parts (e.g. Ball *et al.*, 1993; Lu *et al.*, 2009) but also that the top and the base of a single leaf may differ in frequency of different phytolith morphotypes (Mulholland *et al.*, 1988). Phytolith variation amongst leaves may be influenced by the ages of individual leaves, e.g. older leaves may carry more mature phytoliths than younger ones – similarly to apical (older in grasses) leaf parts compared with basal (younger) parts of the same leaf (Kumar *et al.* 2017). This particularly applies to grasses, where the high variation of phytolith shape within leaves plausibly corresponds to the shape variation of GSSC (e.g. Rudall *et al.*, 2014; Kumar *et al.*, 2017). The phytoliths produced within GSSC would then possibly be typified by a continuous variation of their shape characteristics.

The standard methods used in phytolith analysis are based on the qualitative identification of pre-defined morphotypes {International Code for Phytolith Nomenclature 2.0 [International Committee for Phytolith Taxonomy (ICPT), 2019]}, and do not reflect continuous variation in phytolith shape (although measurements of shape and size may be included). The transitional forms, which do not fit into any defined category, are neglected, or the researchers need to define many different subgroups to capture their subtle shape variations. The challenges facing this typological approach have been discussed in several studies (e.g. Rovner, 2004): (1) similar phytolith morphotypes occur across different species; (2) the complex morphological variation of phytolith shape is reduced to a limited number of subjective morphotypes with vague boundaries between them; and (3) the application of phytolith morphotype nomenclature is inconsistent between various studies. Here, the morphometric approach seems crucial to disentangle the sources of variation in phytoliths, as it can facilitate the quantitative analysis of both the shape and size variation based on measurements of certain morphometric parameters of size and shape (Rovner and Russ, 1992; Ball *et al.*, 2009, 2016; Out *et al.*, 2014; Out and Madella, 2016, 2017). In the case of high intraspecific variation, for example between populations, interspecific differences may be concealed. However, morphometric analysis has proven to be a valuable tool for distinguishing between phytoliths produced by different, sometimes even closely related species: wheat and barley (Ball *et al.*, 1996, 1999), oat (Portillo *et al.*, 2006) and millet species (Out and Madella, 2016; Ge *et al.*, 2018; Zhang *et al.*, 2018). More sophisticated geometric morphometric methods (GMMs) could bring further advances in phytolith analysis and provide levels of taxonomic accuracy which are usually not achieved by traditional approaches (Evett and Cuthrell, 2016; Portillo *et al.*, 2019). A key characteristic of GMMs is that the geometric relationships of studied objects are captured and preserved throughout the subsequent analyses (e.g. Zelditch *et al.*, 2012). A large amount of information about phytolith shape can be obtained from one sampled outline compared with traditional morphometric approaches, and the variation in phytolith size can be subjected to subsequent analyses. Graphical representations resulting from the analyses also enable the exploration of the phytolith shape morphospace.

In this study, we aimed to decompose different sources of phytolith shape and size variation and to evaluate their relative importance in two closely related grass species of tribe Brachypodieae, subfamily Pooideae. We analysed relative proportions of variation explained by differences between (1) species, (2) populations, (3) individual plants, (4) leaves and, finally, (5) segments of leaves. We also asked whether younger and older leaves of the same plant (and even the younger and older parts of the same leaf) differed in their phytolith shape and size. The chosen taxa were the light-demanding, dry-tolerant heath false brome (*Brachypodium pinnatum*), which grows mainly in grassland habitats, and the shade-tolerant wood false brome (*B. sylvaticum*), growing preferentially in forests.

We used landmark-based GMMs (e.g. Zelditch *et al.*, 2012; for more details, see the Materials and Methods). To our knowledge, the landmark-based approach has never been applied to phytoliths. This may stem from the fact that phytoliths are often considered as objects without any readily identifiable or fixed landmarks. Indeed, phytolith outlines do not have many 'anatomical' features that can be used for defining fixed landmarks. However, semi-landmarks, a series of points along the outline which can be slid to achieve corresponding positions according to a chosen criterion (Bookstein, 1997; Gunz and Mitteroecker, 2013), can be used in this situation and were employed in the present study using a methodology generalized for objects with biradial symmetry (Savriama *et al.*, 2010; Savriama and Klingenberg, 2011).

MATERIALS AND METHODS

Material

The study included three populations of two closely related grass species (*Brachypodium pinnatum* and *B. sylvaticum*)

collected in the field at various localities in the Czech Republic and Poland (see Supplementary data Table S1). We collected two individuals per population, keeping several (5–10) metres distance between them. On each site, we recorded the species composition of surrounding vegetation to assess, based on the species demands, the approximate environmental conditions (using the Ellenberg indicator values; Chytrý *et al.*, 2018).

Plant material processing

Plant material was processed following the *in situ* charring method of Kumar *et al.* (2017). This method preserves the original phytolith position within the plant epidermis and allows the analysis of phytoliths in specific leaf parts. Two leaves per plant were sampled: the oldest leaf (basal leaf) was labelled leaf 1 and the youngest leaf was labelled leaf 2. Leaves were cleaned in an ultrasonic cleaner (Digital Ultrasonic Cleaner CE-7200A). The grass leaf epidermal cell division zone is restricted to the base of the developing leaf and, when the newly divided cells elongate, they push the older cells upwards (Skinner and Nelson, 1995). Thus, we sampled the basal (the younger segment 1) and upper (the older segment 2) parts. Segments of leaves were laid on a glass slide (with random orientation regarding abaxial–adaxial leaf sides). Small pieces of folded aluminium foil were placed near the two shorter sides of the slide. Another glass slide was placed on top of the slide, holding the sample in place. We put the slides into a muffle furnace at 330 °C for 3 h. The aluminium foil between the slides prevented the slides from sticking together. We washed the slides containing burnt material with 1 N HCl and distilled water (using a pipette). After the slides dried, we covered plant material placed on the bottom slide with one drop of a 15 % solution of glycerol and then replaced the cover slide. We then subjected the slides to transmission light microscopy (Leica DM 1000 LED).

Phytolith morphotype counts

Additionally, one leaf per population was prepared to obtain traditional phytolith morphotype counts that characterize the species under study. Leaves were cleaned in an ultrasonic cleaner (Digital Ultrasonic Cleaner CE-7200A), then placed in ceramic crucibles and charred in the muffle furnace at 500 °C for 4 h, following Albert *et al.* (1999). Samples were subjected to transmission light microscopy (Leica DM 1000 LED). Phytoliths were classified morphologically according to their shape, following the International Code for Phytolith Nomenclature 2.0 [International Committee for Phytolith Taxonomy (ICPT) 2019]. Three GSSC phytolith morphotypes, named bilobate, polylobate and rondel, were observed and counted in both species under study (see Supplementary data Table S2).

Data acquisition

Sequential microphotographs of rows of GSSC phytoliths in charred epidermis were acquired under ×400 magnification (Leica camera ICC50 W; Fig. 1A–D). For each individual phytolith image (2400 in total), 100 two-dimensional points were digitized. First, two fixed landmarks were placed at the phytolith edges (Fig. 1E). We took into consideration the orientation of the phytolith towards the longest axis of the leaf and placed landmarks on the phytolith edges perpendicular to the longest axis of the leaf. Then, 49 equidistant points were placed along both outline halves, resulting in 98 points which were treated as semi landmarks in the subsequent geometric morphometric analysis. This approach was unambiguously applied to bilobates and polylobates, whereas rondels, positioned from the upper view in leaf epidermis, had no identifiable landmarks and were not analysed. Digitization was carried out using the semi-automated background curves tool in TpsDig, ver. 2.31 (Rohlf, 2015). Equidistant positions of semi-landmarks along

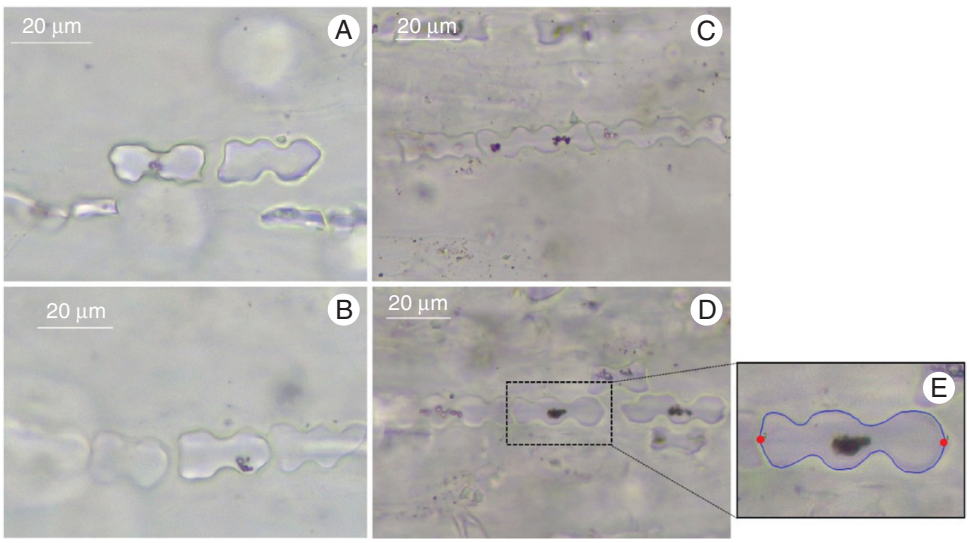

FIG. 1. Microphotographs of *in situ* charred grass epidermis showing phytolith shape morphology variation in *Brachypodium pinnatum* (A, B) and *Brachypodium sylvaticum* (C, D). Phytolith with digitized landmarks (E): two fixed landmarks (red points) and 98 equidistant semi landmarks (49 points along both halves of the phytolith) (blue curves).

the outlines relative to the positions of the fixed landmarks were obtained using the digit.curves function in the geomorph package, ver. 3.0.5 (Adams and Otárola-Castillo, 2013), in R, ver. 3.4.4 (R Core Team, 2018) (for more details, see Supplementary data Table S3).

Data analysis

Generalized Procrustes analysis (GPA) of phytoliths with biradial symmetry. Geometric morphometric analysis was performed on a data set of 2400 phytolith configurations, each consisting of 100 equidistant semi-landmark coordinates. The GPA, which minimizes the sum of squared distances between corresponding landmarks to extract shape data by removing the extraneous information of size, location and orientation, was applied (e.g. Zelditch *et al.*, 2012; Dryden and Mardia, 2016). GPA involved an additional step, allowing the semi-landmarks to slide iteratively along the outline tangents so that their final position yielded the smoothest possible deformation of the actual configuration from the mean shape configuration of the analysed data set. This position is characterized by the lowest possible bending energy between the mean shape and each configuration (Bookstein, 1997; Pérez *et al.*, 2006). The central points in both apical parts of the phytolith sides were treated as fixed landmarks, and 49 points in between along each side of the analysed objects were treated as semi landmarks.

To achieve correspondence of all phytolith configurations under study, we applied GMMs for the analyses of biradial symmetry (Savriama *et al.*, 2010; Savriama and Klingenberg, 2011; Neustupa, 2013). Original phytolith configurations were transformed and relabelled, and then subjected to GPA (Fig. 2; Supplementary data Table S3). The resulting multiplied data set consisted of Procrustes co-ordinates of original configurations and transformed and relabelled copies (a reflected copy about the horizontal adaxial–abaxial axis; a reflected copy about the vertical left–right axis; and a copy reflected about both axes) (Savriama and Klingenberg, 2011; Klingenberg, 2015; Savriama, 2018). By averaging of the original configuration and transformed copies of each specimen, we obtained the consensus (mean) phytolith configurations, which were symmetric and thus invariant under all transformations (Fig. 2C; Supplementary data Table S3). The GPA was conducted using the procGPA function in the geomorph package, ver. 3.0.5 and the shapes package, ver. 1.2.3 in R, ver. 3.4.4 (R Core Team, 2018).

Quantification of components of symmetric and asymmetric variation. Subsequently, principal component analysis (PCA) was conducted on the superimposed Procrustes co-ordinates of the data set consisting of all the original configurations and their transformed copies. This PCA separated components of symmetric shape variation (variation between consensus configurations) from three components of asymmetry (asymmetry under reflection in the adaxial–abaxial direction, asymmetry in the left–right direction and asymmetry regarding both these axes) (Savriama *et al.*, 2010; Klingenberg, 2015). The proportion of variation in sub-spaces of total symmetry and three asymmetric patterns were quantified by summing up the percentages of variance explained by PCs belonging to a given sub-space. The PCA was conducted in the geomorph package ver. 3.0.5 (Adams and Otárola-Castillo, 2013) in R, ver. 3.4.4 (R Core Team, 2018). The most important axes spanning symmetric and asymmetric variation in the shape of individual species were illustrated by deformation grids in PAST, ver. 3.20 (Hammer *et al.*, 2001).

Quantification of different sources of shape and size variation. Different sources of the shape and size variation among phytoliths were quantified by Procrustes analysis of variance (ANOVA) of the consensus configurations and centroid sizes (e.g. Klingenberg, 2015). Data were analysed in a nested structure that was reflected by the Procrustes ANOVA models, with species as the main effect and populations, plants, leaves and segments of leaf as random nested effects. The nested structure of the data required the appropriate construction of the *F*-ratios in the model; thus, the mean squares (MS) of the main effect of 'species' were divided by the MS of the nested factor, i.e. population. Likewise, the MS of 'population' were divided by the MS of 'plants' to yield the *F*-ratio for the 'population' factor, etc. The *P*-values denoting level of significance of the effects in the model were established by comparing *F*-values obtained for each factor with those obtained by 999 random permutation of the shape and size data.

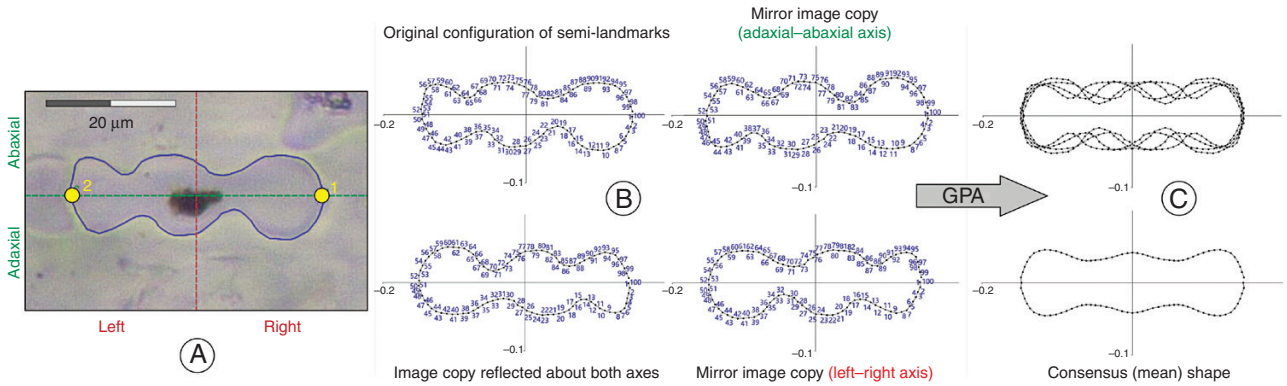

FIG. 2. Workflow sequence of landmark-based geometric morphometrics performed on phytoliths with biradial symmetry. (A) Digitation of landmarks. (B) Reflection and relabelling of semi-landmarks. Relabelling is required to ensure that original configuration and transformed copies match. (C) GPA performed on the multiplied data set. The consensus (mean) configurations (obtained by averaging of original and transformed configurations) are invariant under all transformation.

Exploration of morphospace of Brachypodium species and classification of species based on their phytolith shape. The PCA was performed on the consensus phytolith configurations, and shape variations associated with individual PCs were illustrated by deformation grids. To test whether individual phytoliths can be assigned to one of two pre-defined species groups, linear discriminant analysis (LDA) was conducted in order to discriminate between species based on phytolith shape. From multiple measures on two different species, LDA seeks a linear combination (the discriminant function) that maximizes the ratio of the between-group sum of squares to the within-group sum of squares (e.g. Mitteroecker and Bookstein, 2011). A specimen with unknown group affiliation can be assigned to one or the other of the two groups based on its score for this linear combination. Here, variables (Procrustes co-ordinates) were reduced by PCA of the consensus phytolith shape variation prior to LDA. Thus, LDA was based on the first 34 PCs (each component explaining >0.001 % of total variation). The analysis yielded the discriminant function which, applied to the data set again, resulted in the proportion of correctly classified (or misclassified) individual phytoliths. Both PCA and LDA were conducted in PAST, ver. 3.20 (Hammer *et al.*, 2001).

RESULTS

Decomposition of symmetric and asymmetric variation in phytolith shape

The PCA of the multiplied data set yielded PCs which were further partitioned into several groups of components bearing either symmetric or asymmetric shape variation (Fig. 3). The first group of PCs, associated exclusively with symmetric shape variation (between the consensus phytolith configurations), accounted for 68.7 % of the total variation of the data set. For example, the shape variation associated with PC1 differentiated between phytoliths with three (or more) deeply incised lobes against shapes with just two shallow lobes in opposite directions. The second group of PCs, associated with asymmetric shape variation, accounted for 26.1 % of the total variation. Thus, the PCA results indicated that phytolith shape variation consisted mainly of symmetric variation. Therefore, in the following analyses of phytolith shape, we took into consideration only the data set of the consensus phytolith configurations.

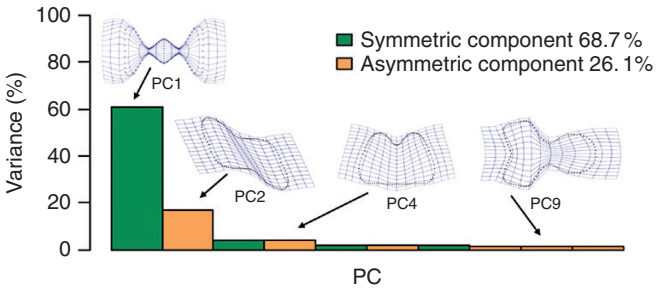

Fig. 3. Proportion of phytolith shape variation in the multiplied data set along principal components (PCs). Each of ten PCs is associated with either symmetric or asymmetric shape variation. PC1, symmetric component; PC2, asymmetry under reflection about either of the two axes but symmetric by 180° rotation; PC4, asymmetry under reflection about the adaxial–abaxial direction with left–right symmetry; PC9, asymmetry in the left–right direction but with adaxial–abaxial symmetry.

Inter- and intraspecific variation in both the shape and size of phytoliths

Different sources of inter- and intraspecific variation accounted for 49 % of the total variation in phytolith consensus shape (Fig. 4; Supplementary data Table S4), with interspecific variation being the most pronounced (34 %, $P = 0.001$). Intraspecific variation was, on the other hand, considerably lower (15 %). The variation among different populations of the same species accounted for just 2.7 % of total variation, whereas differences among individual samples spanned about 3.1 % of total variation. The variation among individual plants and leaves was slightly higher (4.3 and 4.9 % of total variation, respectively). In addition, we related intraspecific variation in phytolith shape with phases of plant ontogeny. Specifically, we tested the variation between younger and older leaves and between younger and older parts of the leaves. The overall variation in shape relating to plant ontogeny was very low (2.0 %). However, phytoliths were slightly elongated in older leaves (Supplementary data Tables S5 and S6).

We also evaluated different sources of variation in phytolith size (Fig. 4; Supplementary data Table S7). Together, different sources of inter- and intraspecific variation in phytolith size accounted for 48 % of total variation in the data set. However, concerning interspecific variation, the variation in phytolith size was considerably lower (18 %) than variation in phytolith shape (34 %, see above). Overall, in phytolith size, intraspecific variation was higher compared with interspecific variation (28 and 18 %, respectively), with the variation among populations of the same species being lower (4.8 %) than the variation between individual samples (4.9 %) and leaves (6.6 %). The highest variation in phytolith size was between individual plants of the same species (11.9 %). The variation in size relating to plant ontogeny was very low (2.4 %); however,

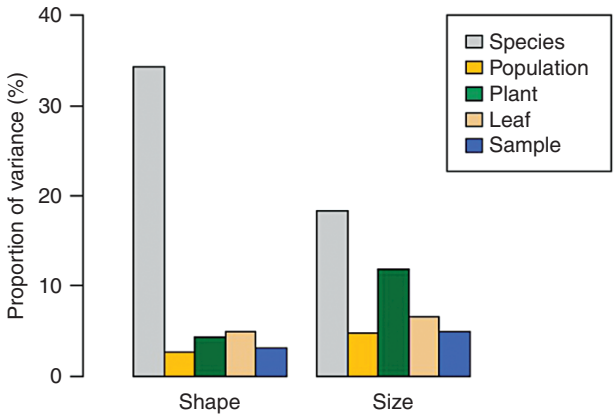

Fig. 4. Proportion of inter- and intraspecific variation in phytolith shape (left) and size (right). In shape, interspecific variation (34 %) outweighed total intraspecific variation (15 %), while in size, interspecific variation was lower (18 %) compared with total intraspecific variation (28 %), with the highest variation between plants (12 %). Therefore, phytolith shape was crucial for discriminating between the species.

phytoliths were slightly bigger in older leaves (Supplementary data Tables S8 and S9).

The exploration of phytolith morphospace of Brachypodium species

The PCA uncovered the most pronounced variation in phytolith consensus shapes. According to the PCA performed on symmetric variation of the consensus configurations, the first two PCs explained >93 % of the total variation (Fig. 5). Along PC1 (explaining 87.8 % of the total variation), phytoliths varied between elongated shapes with three (or more) deeply incised lobes (polylobates associated mainly with *B. sylvaticum*), and shorter, almost equidimensional, shapes with two lobes on opposite sides (bilobates associated mainly with *B. pinnatum*). Along PC2 (explaining 5.3 % of the total variation), phytolith shape varied between elongated outlines with two deeply incised lobes and shorter shapes without distinct lobes on the opposite sides. The variation along PC2 was noticeably higher for positive values of PC1, where mainly bilobates occurred; the variation in polylobates, for negative values of PC1, was considerably more uniform. The phytoliths with two, distinctly incised lobes occurred mainly around the centre of the diagram (particularly for positive values of PC2), displaying a shape shared by both species (neither elongated nor short).

Classification of phytoliths from Brachypodium species

Based on the previous results, we tried to classify the two studied *Brachypodium* species solely according to their consensus phytolith shapes. The LDA, based on 34 PCs, led to 83 % of classifications of individual phytoliths being correct; *B. pinnatum* was correctly classified in 85 % of cases and *B. sylvaticum* in 81 % of cases (Fig. 6). Misclassification of some phytoliths (17 % of cases) was due to the fact that the species partly overlapped in their phytolith shapes; in other words, some shapes were more redundant than the others. For each species, we identified the most informative phytolith consensus shapes, with respect to their identification, which were those being the most common in a given species and having a relatively low proportion of misclassifications at the same time (Fig. 6). This is in accordance with the results of traditional morphotype counts, which showed a higher frequency of polylobates in *B. sylvaticum*, and bilobates in *B. pinnatum* (see Supplementary data Table S2).

DISCUSSION

Summary

In this study of two grass species, we showed that interspecific variation largely outweighed intraspecific variation with respect to phytolith shape. This implies that, at least in some cases, variation in phytolith shape may be crucial in discriminating between species. Our outline analysis – based on semi-landmark Procrustes superimposition – was applied to phytoliths for the first time. It enabled the evaluation of different sources of phytolith shape variation and subsequently the classification of phytoliths of both grass species.

Application of geometric morphometric methods in phytolith analysis

We encountered one of the major issues of the typological approach – specifically, that similar phytolith morphotypes occur across different species (redundancy) – when we found, in our pooid *Brachypodium* species, bilobates and polylobates which are commonly ascribed to panicoids (Twiss *et al.*, 1969, 1992; Fredlund and Tieszen, 1994; Bremond *et al.*, 2005). We acknowledge that the problem of morphotype redundancy could be overcome by defining various sub-categories using detailed descriptions (e.g. Fahmy, 2008; Barboni and Bremond, 2009).

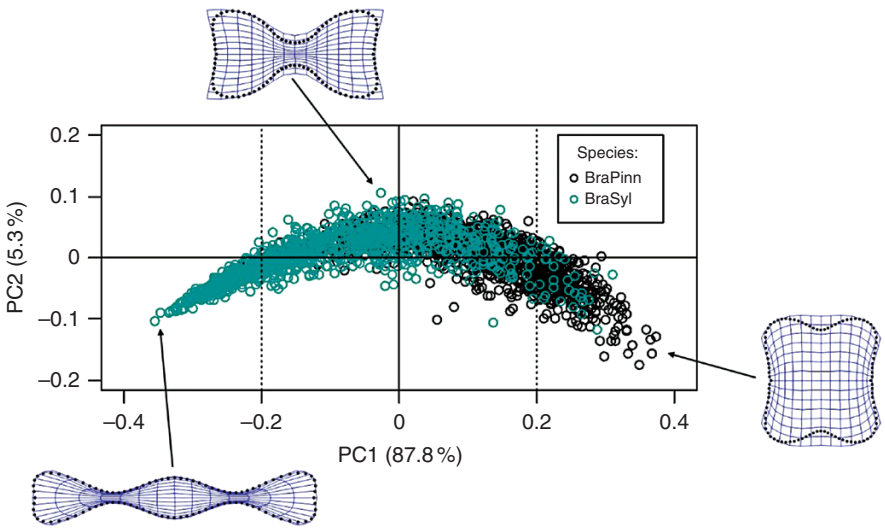

FIG. 5. Variation in phytolith consensus shape analysed by principal component analysis (PCA). BraPinn, *Brachypodium sylvaticum* (blue circles); BraSyl, B. *pinnatum* (black circles).

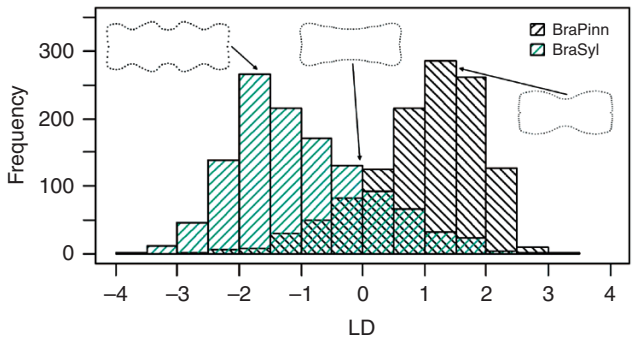

FIG. 6. Classification of phytoliths using the linear discriminant analysis of their consensus shapes. Frequency of correctly classified phytoliths scoring on the linear discriminant function (LD): BraPinn, *Brachypodium pinnatum*; BraSyl, B. *sylvaticum*. Shapes scoring around zero were equally common in both species, which caused their overlap (black and blue shaded lines crossed) and resulted in 17 % of misclassifications. Phytolith shapes being the most informative, with respect to species identification, were those scoring between one and two (same in negative values) – they were the most common in a given species and had a relatively low proportion of misclassifications at the same time.

However, the use of additional descriptors compounds the issue of consistency among laboratories and hampers the comparison of results. In this study, we attempted to build on efforts to overcome this problem by utilizing landmark-based GMMs (and semi-landmark Procrustes superimposition in particular). Compared with the morphometric parameters that are traditionally used, GMMs capture the whole geometry of a phytolith and retain this information throughout subsequent analyses (Adams *et al.*, 2013).

It should be noted that the Procrustes superimposition of phytolith shapes may not be universally applicable to all known morphotypes occurring in natural samples. The Procrustes registration critically relies on the point-to-point correspondence of individual semi landmarks among the analysed specimens. Even in the situation where an entire outline of a studied specimen is taken as a single curve spanned by a series of equidistant semi landmarks, there is a necessity for a starting point, the position of which needs to correspond biologically across specimens. As shown in this study, in phytoliths with symmetric 2-D shapes, there may be two or more fixed points delimiting individual symmetric curves. These points are typically derived from the orientation of phytoliths within plant tissue (we note that this does not imply that the whole epidermis must be preserved to unambiguously place landmarks on fossil phytoliths; however, some knowledge about phytolith orientation within plant tissue is required). Besides bilobates and polylobates, this applies to the long row of additional morphotypes such as saddles, crenates, trapezoids and complex forms of elongates from grass inflorescence bracts. However, phytoliths that do not bear any such corresponding points, such as those classified into rondel or spheroid groups, would be unsuitable for a clear-cut morphometric analysis by GPA. In these cases, correspondence among the specimens can only be achieved by purely geometric registration, such as that based on the ellipse of the first harmonic function of elliptic Fourier analysis (Kuhl and Giardina, 1982). Such analysis can then involve a variety of phytolith shapes that can be successfully distinguished among groups (Cai and Ge, 2017), though, obviously, it cannot involve any separation of symmetric and asymmetric components due to a lack of correspondence among the outlines. This appeared especially useful in this study, where our results provoked a greater interest in symmetric variation in subsequent analyses, particularly with respect to discriminating between species. However, we recommend testing the relevance of asymmetric variation (e.g. for studying the relationships between phytolith asymmetry and environmental conditions).

'Quasi-horseshoe' pattern in geometric morphometric data

Recently, it has been pointed out that in geometric morphometric data with high dimensionality (such as the dense series of semi-landmarks used in this study), PC2 usually contracts the middle of the shape variation series (typically spanned by PC1) with both of its ends (Polly and Motz, 2016). This leads to seemingly 'horseshoe'-shaped ordination plots of these two PCs. This pattern is invariably produced by high dimensional GMM data, even if the co-ordinates are modelled by Brownian motion random walks (Polly and Motz, 2016). In fact, it was shown that the predictability of this effect increases with the number of variables, such as the number of semi-landmarks along the analysed outlines (Bookstein, 2013), and in analyses of data involving any gradational series, such as segmental structures (Bastir *et al.*, 2019). Obviously, this might also have been the cause of the similar pattern produced by PC1 and PC2 in our analysis. However, it should be pointed out that this phenomenon does not invalidate the morphospace structure represented by PCA (Polly and Motz, 2016), because the shape distances among the specimens are preserved in the multidimensional shape space represented by a sequence of multiple PCs. Conversely, any use of 'corrections' to this phenomenon, such as detrended correspondence analysis, would lead to undesirable distortions of the shape space. However, it should be stressed that subsequent morphospace analyses have to use multidimensional data contained in the series of multiple PCs representing the true pattern of the shape differences among specimens (Polly and Motz, 2016), which is what we used in LDAs conducted in the course of our analyses.

Intraspecific variation in phytolith shape and size

In the current study, we only compared two grass species in order to demonstrate our approach on a simplified system. Nevertheless, we paid special attention to different sources of intraspecific variation in phytolith shape and size and used geometric morphometrics to quantify them in a large data set of 2400 phytoliths. According to our results, intraspecific variation in phytolith consensus shapes was much lower than interspecific variation (while in the case of phytolith size, intraspecific variation was slightly higher than the interspecific kind). Surprisingly, we observed that phytolith shape and size varied the least between populations. In addition, the variation explained by the ages of leaves or their parts was also very low in both phytolith shape and size (no more than 2.4 % of explained variation), although phytoliths in older leaves were

significantly larger than those in younger leaves. This agrees with the previous study by Rovner and Russ (1992) showing that phytolith shape and size are not affected by the location of phytoliths within leaves. However, the relatively high residual variation (51 % of total variation) can be ascribed to the high plasticity of phytolith shape within each sample. This means that phytoliths vary continually within a section of leaf epidermis and, therefore, that individual phytoliths in a single sample may differ more from each other than from those which originated in other species. Such plasticity within individual samples is therefore more responsible for the overlap between species than any other source of variation.

Since the variation between populations of the same species was very low, we did not demonstrate any relationship between phytolith variation and environmental conditions. We know from other studies that phytoliths can be larger in humid conditions than in arid ones (Liu *et al.*, 2016). However, according to other studies, phytolith shape seems to remain constant under varying environmental conditions (Ball and Brotherson, 1992). In our study, we collected material in the field and analysed phytoliths of two species with rather restricted ecological niches. A question arises of how phytolith shape and size would vary between populations of a more generalist species growing naturally in contrasting conditions (e.g. *Calamagrostis epigejos*) or in specimens shifted outside their realized niche (in experimental conditions). Dunn *et al.* (2015) showed that some phytolith morphotypes (crenate, polylobate) of various grass species tend to be bigger and relatively longer in experimentally shaded conditions. We acknowledge the need for more studies on this subject. However, we regard our findings of low intraspecific variation in phytolith shape to be an important confirmation of the validity of the use of phytolith analysis in paleoecology.

Phytoliths in fossil records

The application of geometric morphometric analysis has the potential to identify subtle variations in shape not readily apparent to the naked eye and thereby to greatly improve the researcher's ability to discriminate between phytoliths of different species. There is a strong possibility that morphometric approaches to phytolith identification could enable much finer discrimination of plant taxa than previously possible, allowing much better interpretation of past environments than currently possible. In paleoecology, we usually draw conclusions based on phytolith morphotype counts and their distinctive combinations (phytolith spectra), which imply the proportions of certain functional groups (e.g. grasses vs. trees) (e.g. Bremond *et al.*, 2005; Barboni *et al.*, 2007) or vegetation types (e.g. steppe lawns vs. mesophilic meadows) (e.g. Solomonova *et al.*, 2019), rather than rely on species-specific phytoliths to establish the presence of particular species. Here, we demonstrated that it is possible to assign individual phytolith shapes to a specific plant species (our success rate in the two-species model was 83 %). This means that we can supplement the interpretation of fossil phytolith spectra with the probability that its individual phytoliths belong to a particular taxon. This creates a whole new option for interpreting past environments which would complement traditionally used morphotype counts in specific cases.

We expect that this approach will be most useful for the reconstruction of grassland vegetation characterized by the dominance of just a few diagnostic grass species. Grass taxa which have high abundance in a plant community in terms of individuals (e.g. *Phragmites* sp. and *Molinia* sp.) and belong to a subfamily which is represented by only a few species in the investigated area (e.g. Arundinoideae) are the best candidates. In addition, pooid tribes (e.g. Brachypodieae and Stipeae), forming sister groups to the most diverse tribe Poeae (Soreng *et al.*, 2017), hold great potential for further discrimination, as was shown, for example, in Gallego and Distel (2004). However, the reliability of these assumptions must be tested on extensive reference material, using phytoliths coming both from reference material and from surface soils.

Regarding the general applicability of our approach, we do not expect the landmark-based geometric morphometrics of phytoliths to replace other traditional approaches but rather to complement them and make phytolith analysis more accurate in specific cases, as stated above. Nevertheless, the processing of data for analysis is not very time consuming – especially when we take into account the amount of information about shape obtained from one sampled outline compared with traditional morphometric approaches, where measured parameters have to be chosen in advance without knowing whether or not they are relevant for answering the questions asked. Also, the consistent application of qualitatively defined morphotypes can be rather problematic for less-experienced researchers; similarly, to become familiar with all of the classification schemes used by different researchers also takes a considerable amount of time. It is possible that in the future it will prove productive to involve machine learning methods in discrimination of individual phytolith shapes.

Conclusions

Our results suggest that phytolith shape corresponds relatively closely to the taxonomic identity of closely related grass species. Moreover, our methodological approach, applied to phytolith analysis for the first time, enables the quantification and separation of variation that is not related to species discrimination. We believe that our approach can, in the same way, shed light on other topics which are in their infancy, such as attempts to study patterns of phytolith shape variation in a phylogenetic context (Prasad *et al.*, 2011; Rudall, 2014; Strömberg *et al.*, 2018). As shown by the application of geometric morphometrics in many other fields, its application to phytolith analysis will probably raise and answer many completely new questions (Adams *et al.*, 2013).

SUPPLEMENTARY DATA

Supplementary data are available online at https://academic.oup.com/aob and consist of the following. Table S1: the studied plant material and experimental design. Ellenberg indicator

values for light, temperature, moisture, reaction and nutrients. Table S2: phytolith morphotype counts. Table S3: workflow sequence of landmark-based geometric morphometric and other methods used in the current study. Table S4: Procrustes ANOVA evaluating effect of inter- and intraspecific symmetric variation in phytolith consensus shape. Table S5: Procrustes ANOVA evaluating effect of phases of plant ontogeny on phytolith shape. Table S6: Procrustes ANOVA evaluating effect of phases of plant ontogeny on phytolith consensus shape. Table S7: ANOVA evaluating effect of inter- and intraspecific variation in phytolith size. Table S8: ANOVA evaluating effect of phases of plant ontogeny on phytolith size. Table S9: ANOVA evaluating effect of phases of plant ontogeny leaf part age) on phytolith size.

ACKNOWLEDGEMENTS

We thank Professor Tomáš Herben and Doctor Patrik Mráz, and all participants of the course: 'Scientific writing in plant ecology and evolution' realized at the Department of Botany, Charles University in Prague for helpful comments on initial versions of the manuscript. We would like to thank both anonymous referees for their valuable and knowledgeable comments on the final manuscript. We thank Matthew Nicholls for his diligent proofreading of the final manuscript, and Jan Hošek for his graphical suggestions.

FUNDING

This work was supported by the Czech Science Foundation project [17-07851S].

LITERATURE CITED

Adams DC, Otárola-Castillo E. 2013. *geomorph*: an R package for the collection and analysis of geometric morphometric shape data. *Methods in Ecology and Evolution* **4**: 393–399.

Adams DC, Rohlf FJ, Slice DE. 2013. A field comes of age: geometric morphometrics in the 21st century. *Hystrix, the Italian Journal of Mammalogy* **24**: 7–14

Albert RM, Lavi O, Estroff L, Weiner S. 1999. Mode of occupation of Tabun Cave, Mt Carmel, Israel during the Mousterian period: a study of the sediments and phytoliths. *Journal of Archaeological Science* **26**: 1249–1260.

Alexandre A, Meunier JD, Lezine AM, Vincens A, Schwartz D. 1997. Phytoliths: indicators of grassland dynamics during the late Holocene in intertropical Africa. *Palaeogeography, Palaeoclimatology, Palaeoecology* **136**: 213–232.

Ball TB, Brotherson JD. 1992. The effect of varying environmental conditions on phytolith morphometries in two species of grass (*Bouteloua curtipendula* and *Panicum virgatum*). *Scanning Microscopy* **6**: 1163–1181.

Ball TB, Brotherson JD, Gardner JS. 1993. A typologic and morphometric study of variation in phytoliths from einkorn wheat (*Triticum monococcum*). *Canadian Journal of Botany* **71**: 1182–1192.

Ball TB, Gardner JS, Brotherson JD. 1996. Identifying phytoliths produced by the inflorescence bracts of three species of wheat (*Triticum monococcum* L., *T. dicoccon* Schrank., and *T. aestivum* L.) using computer-assisted image and statistical analyses. *Journal of Archaeological Science* **23**: 619–632.

Ball TB, Gardner JS, Anderson N. 1999. Identifying inflorescence phytoliths from selected species of wheat (*Triticum monococcum*, *T. dicoccon*, *T. dicoccoides*, and *T. aestivum*) and barley (*Hordeum vulgare* and *H. spontaneum*) (Gramineae). *American Journal of Botany* **86**: 1615–1623.

Ball TB, Ehlers R, Standing MD. 2009. Review of typologic and morphometric analysis of phytoliths produced by wheat and barley. *Breeding Science* **59**: 505–512.

Ball TB, Davis A, Evett RR, *et al.* 2016. Morphometric analysis of phytoliths: recommendations towards standardization from the International Committee for Phytolith Morphometrics. *Journal of Archaeological Science* **68**: 106–111.

Barboni D, Bremond L. 2009. Phytoliths of East African grasses: an assessment of their environmental and taxonomic significance based on floristic data. *Review of Palaeobotany and Palynology* **158**: 29–41.

Barboni D, Bremond L, Bonnefille R. 2007. Comparative study of modern phytolith assemblages from inter-tropical Africa. *Palaeogeography, Palaeoclimatology, Palaeoecology* **246**: 454–470.

Barboni D, Ashley GM, Dominguez-Rodrigo M, Bunn HT, Mabulla AZP, Baquedano E. 2010. Phytoliths infer locally dense and heterogeneous paleovegetation at FLK North and surrounding localities during upper Bed I time, Olduvai Gorge, Tanzania. *Quaternary Research* **74**: 344–354.

Bastir M, Torres-Tamayo N, Palancar CA, *et al.* 2019. Geometric morphometric studies in the human spine. In: Been E, Gómez-Olivencia A, Ann Kramer P, eds. *Spinal evolution*. Cham: Springer, 361–386.

Blinnikov MS, Busacca A, Whitlock C. 2002. Reconstruction of the Late Pleistocene grassland of the Columbia basin, Washington, USA, based on phytolith records in loess. *Palaeogeography, Palaeoclimatology, Palaeoecology* **177**: 77–101.

Bookstein FL. 1997. Landmark methods for forms without landmarks: morphometrics of group differences in outline shape. *Medical Image Analysis* **1**: 225–243.

Bookstein FL. 2013. Random walk as a null model for high-dimensional morphometrics of fossil series: geometrical considerations. *Paleobiology* **39**: 52–74.

Bremond L, Alexandre A, Hély C, Guiot J. 2005. A phytolith index as a proxy of tree cover density in tropical areas: calibration with leaf area index along a forest–savanna transect in southeastern Cameroon. *Global and Planetary Change* **45**: 277–293.

Cai Z, Ge S. 2017. Machine learning algorithms improve the power of phytolith analysis: a case study of the tribe Oryzeae (Poaceae). *Journal of Systematics and Evolution* **55**: 377–384.

Chytrý M, Tichý L, Dřevojan P, Sádlo J, Zelený D. 2018. Ellenberg-type indicator values for the Czech flora. *Preslia* **90**: 83–103.

Cooke J, Leishman MR. 2011. Is plant ecology more siliceous than we realise? *Trends in Plant Science* **16**: 61–68.

Delhon C, Alexandre A, Berger JF, Thiebault S, Brochier JL, Meunier JD. 2003. Phytolith assemblages as a promising tool for reconstructing Mediterranean Holocene vegetation. *Quaternary Research* **59**: 48–60.

Dryden IL, Mardia KV. 2016. *Statistical shape analysis: with applications in R*, Vol. **995**. Chichester: John Wiley & Sons.

Dunn RE, Le TY, Strömberg CA. 2015. Light environment and epidermal cell morphology in grasses. *International Journal of Plant Sciences* **176**: 832–847.

Epstein E. 2009. Silicon: its manifold roles in plants. *Annals of Applied Biology* **155**: 155–160.

Evett RR, Bartolome JW. 2013. Phytolith evidence for the extent and nature of prehistoric Californian grasslands. *The Holocene* **23**: 1644–1649.

Evett RR, Cuthrell RQ. 2013. Phytolith evidence for a grass-dominated prairie landscape at Quiroste Valley on the Central Coast of California. *California Archaeology* **5**: 319–335.

Evett RR, Cuthrell RQ. 2016. A conceptual framework for a computer-assisted, morphometric-based phytolith analysis and classification system. *Journal of Archaeological Science* **68**: 70–78.

Fahmy AG. 2008. Diversity of lobate phytoliths in grass leaves from the Sahel region, West Tropical Africa: tribe Paniceae. *Plant Systematics and Evolution* **270**: 1–23.

Fredlund GG, Tieszen LT. 1994. Modern phytolith assemblages from the North American great plains. *Journal of Biogeography* **21**: 321–335.

Fredlund GG, Tieszen LL. 1997. Phytolith and carbon evidence for Late Quaternary vegetation and climate change in the Southern Black Hills, South Dakota. *Quaternary Research* **47**: 206–217.

Gallego L, Distel RA. 2004. Phytolith assemblages in grasses native to central Argentina. *Annals of Botany* **94**: 865–874.

Ge Y, Lu H, Zhang J, Wang C, He K, Huan X. 2018. Phytolith analysis for the identification of barnyard millet (*Echinochloa* sp.) and its implications. *Archaeological and Anthropological Sciences* **10**: 61–73.

Gunz P, Mitteroecker P. 2013. Semilandmarks: a method for quantifying curves and surfaces. *Hystrix, the Italian Journal of Mammalogy* **24**: 103–109.

Hammer Ø, Harper DAT, Ryan PD. 2001. PAST: paleontological statistics software package for education and data analysis. *Palaeontologia Electronica* **4**: 9.

Hart TC. 2016. Issues and directions in phytolith analysis. *Journal of Archaeological Science* **68**: 24–31.

Hodson MJ, White PJ, Mead A, Broadley MR. 2005. Phylogenetic variation in the silicon composition of plants. *Annals of Botany* **96**: 1027–1046.

International Committee for Phytolith Taxonomy (ICPT). 2019. International code for phytolith nomenclature (ICPN) 2.0. *Annals of Botany* **124**: 189–199.

Katz O. 2015. Silica phytoliths in angiosperms: phylogeny and early evolutionary history. *New Phytologist* **208**: 642–646.

Katz O. 2019. Silicon content is a plant functional trait: implications in a changing world. *Flora* **254**: 88–94.

Katz O, Lev-Yadun S, Bar P. 2013. Plasticity and variability in the patterns of phytolith formation in *Asteraceae* species along a large rainfall gradient in Israel. *Flora* **208**: 438–444.

Klingenberg CP. 2015. Analyzing fluctuating asymmetry with geometric morphometrics: concepts, methods, and applications. *Symmetry* **7**: 843–934.

Kuhl FP, Giardina CR. 1982. Elliptic Fourier features of a closed contour. *Computer Graphics and Image Processing* **18**: 236–258.

Kumar S, Milstein Y, Brami Y, Elbaum M, Elbaum R. 2017. Mechanism of silica deposition in sorghum silica cells. *New Phytologist* **213**: 791–798.

Liu L, Jie D, Liu H, *et al.* 2016. Response of phytoliths in *Phragmites australis* to environmental factors in northeast China. *Ecological Engineering* **92**: 119–131.

Lu H, Liu KB. 2003. Morphological variations of lobate phytoliths from grasses in China and the south-eastern United States. *Diversity and Distributions* **9**: 73–87.

Lu H, Zhang J, Wu N, Liu KB, Xu D, Li Q. 2009. Phytoliths analysis for the discrimination of Foxtail millet (*Setaria italica*) and Common millet (*Panicum miliaceum*). *PLoS One* **4**: e4448.

Madella M, Jones MK, Echlin P, Powers-Jones A, Moore M. 2009. Plant water availability and analytical microscopy of phytoliths: implications for ancient irrigation in arid zones. *Quaternary International* **193**: 32–40.

McCune JL, Vellend M, Pellatt MG. 2015. Combining phytolith analysis with historical ecology to reveal the long-term, local-scale dynamics within a savannah–forest landscape mosaic. *Biodiversity and Conservation* **24**: 609–626.

Metcalfe CR. 1960. *Anatomy of the monocotyledons. I. Gramineae*. Oxford: Clarendon Press.

Mitteroecker P, Bookstein F. 2011. Linear discrimination, ordination, and the visualization of selection gradients in modern morphometrics. *Evolutionary Biology* **38**: 100–114.

Mulholland SC, Rapp G. eds. 1992. A morphological classification of grass silica-bodies. In: *Phytolith systematics*. Boston: Springer, 65–89.

Mulholland SC, Rapp G Jr, Ollendorf AL. 1988. Variation in phytoliths from corn leaves. *Canadian Journal of Botany* **66**: 2001–2008.

Neumann K, Fahmy A, Lespez L, Ballouche A, Huysecom E. 2009. The Early Holocene palaeoenvironment of Ounjougou (Mali): phytoliths in a multiproxy context. *Palaeogeography, Palaeoclimatology, Palaeoecology* **276**: 87–106.

Neustupa J. 2013. Patterns of symmetric and asymmetric morphological variation in unicellular green microalgae of the genus *Micrasterias* (Desmidiales, Viridiplantae). *Fottea* **13**: 53–63.

Out WA, Madella M. 2016. Morphometric distinction between bilobate phytoliths from *Panicum miliaceum* and *Setaria italica* leaves. *Archaeological and Anthropological Sciences* **8**: 505–521.

Out WA, Madella M. 2017. Towards improved detection and identification of crop by-products: morphometric analysis of bilobate leaf phytoliths of *Pennisetum glaucum* and *Sorghum bicolor*. *Quaternary International* **434**: 1–14.

Out WA, Pertusa Grau JF, Madella M. 2014. A new method for morphometric analysis of opal phytoliths from plants. *Microscopy and Microanalysis* **20**: 1876–1887.

Pérez R, De Ciurana J, Riba C. 2006. The characterization and specification of functional requirements and geometric tolerances in design. *Journal of Engineering Design* **17**: 311–324.

Piperno DR. 2006. *Phytoliths: a comprehensive guide for archaeologists and paleoecologists.* Lanham, New York, Toronto, Oxford: AltaMira Press (Rowman & Littlefield).

Polly PD, Motz GJ. 2016. Patterns and processes in morphospace: geometric morphometrics of three-dimensional objects. *The Paleontological Society Papers* **22**: 71–99.

Portillo M, Ball T, Manwaring J. 2006. Morphometric analysis of inflorescence phytoliths produced by *Avena sativa* L. and *Avena strigos* schreb. *Economic Botany* **60**: 121–129.

Portillo M, Ball TB, Wallace M, *et al.* 2019. Advances in morphometrics in archaeobotany. *Environmental Archaeology* **25**: 246–256.

Prasad V, Strömberg CA, Leaché AD, *et al.* 2011. Late Cretaceous origin of the rice tribe provides evidence for early diversification in Poaceae. *Nature Communications* **2**: 480.

Prychid CJ, Rudall PJ, Gregory M. 2003. Systematics and biology of silica bodies in monocotyledons. *The Botanical Review* **69**: 377–440.

R Core Team. 2018. *R: a language and environment for statistical computing.* Vienna, Austria: R Foundation for Statistical Computing.

Renvoize SA. 1987. A survey of leaf-blade anatomy in grasses XI. Paniceae. *Kew Bulletin* **1987**: 739–768.

Rohlf FJ. 2015. The tps series of software. *Hystrix, the Italian Journal of Mammalogy* **26**: 9–12.

Rosen AM. 1992. Preliminary identification of silica skeletons from Near Eastern archaeological sites: an anatomical approach. In: Mulholland SC, Rapp G, eds. *Phytolith systematics*. Boston: Springer, 129–147.

Rovner I. 2004. On transparent blindfolds: comments on identifying maize in Neotropical sediments and soils using cob phytoliths. *Journal of Archaeological Science* **31**: 815–819.

Rovner I, Russ JC. 1992. Darwin and design in phytolith systematics: morphometric methods for mitigating redundancy. In: Mulholland SC, Rapp G, eds. *Phytolith systematics*. Boston: Springer, 253–276.

Rudall PJ, Prychid CJ, Gregory T. 2014. Epidermal patterning and silica phytoliths in grasses: an evolutionary history. *The Botanical Review* **80**: 59–71.

Savriama Y. 2018. A step-by-step guide for geometric morphometrics of floral symmetry. *Frontiers in Plant Science* **9**: 1433.

Savriama Y, Klingenberg CP. 2011. Beyond bilateral symmetry: geometric morphometric methods for any type of symmetry. *BMC Evolutionary Biology* **11**: 280.

Savriama Y, Neustupa J, Klingenberg CP. 2010. Geometric morphometrics of symmetry and allometry in *Micrasterias rotata* (Zygnemophyceae, Viridiplantae). *Nova Hedwigia* **136**: 43–54.

Schoelynck J, Bal K, Backx H, Okruszko T, Meire P, Struyf E. 2010. Silica uptake in aquatic and wetland macrophytes: a strategic choice between silica, lignin and cellulose? *New Phytologist* **186**: 385–391.

Shillito LM. 2013. Grains of truth or transparent blindfolds? A review of current debates in archaeological phytolith analysis. *Vegetation History and Archaeobotany* **22**: 71–82.

Skinner RH, Nelson CJ. 1995. Elongation of the grass leaf and its relationship to the phyllochron. *Crop Science* **35**: 4–10.

Solomonova MY, Blinnikov MS, Silantyeva MM, Speranskaja NY. 2019. Influence of moisture and temperature regimes on the phytolith assemblage composition of mountain ecosystems of the mid latitudes: a case study from the Altay Mountains. *Frontiers in Ecology and Evolution*. doi: 10.3389/fevo.2019.00002.

Soreng RJ, Peterson PM, Romaschenko K, *et al.* 2017. A worldwide phylogenetic classification of the Poaceae (Gramineae) II: An update and a comparison of two 2015 classifications. *Journal of Systematics and Evolution* **55**: 259–290.

Strömberg CA, Di Stilio VS, Song Z. 2016. Functions of phytoliths in vascular plants: an evolutionary perspective. *Functional Ecology* **30**: 1286–1297.

Strömberg CA, Dunn RE, Crifò C, Harris EB. 2018. Phytoliths in paleoecology: analytical considerations, current use, and future directions. In: Croft DA, Su D, Simpson SW, eds. *Methods in Paleoecology*. Cham: Springer, 235–287.

Strömberg CA, Werdelin L, Friis EM, Saraç G. 2007. The spread of grass-dominated habitats in Turkey and surrounding areas during the Cenozoic: phytolith evidence. *Palaeogeography, Palaeoclimatology, Palaeoecology* **250**: 18–49.

Tsartsidou G, Lev-Yadun S, Albert RM, Miller-Rosen A, Efstratiou N, Weiner S. 2007. The phytolith archaeological record: strengths and weaknesses evaluated based on a quantitative modern reference collection from Greece. *Journal of Archaeological Science* **34**: 1262–1275.

Twiss PC. 1992. Predicted world distribution of C 3 and C 4 grass phytoliths. In: Mulholland SC, Rapp G, eds. *Phytolith systematics*. Boston: Springer, 113–128.

Twiss PC, Suess E, Smith RM. 1969. Morphological classification of grass phytoliths 1. *Soil Science Society of America Journal* **33**: 109–115.

Whang S, Kim K, Hess W. 1998. Variation of silica bodies in leaf epidermal long cells within and among seventeen species of *Oryza* (*Poaceae*). *American Journal of Botany* **85**: 461.

Zelditch ML, Swiderski DL, Sheets DH. 2012. *Geometric morphometrics for biologists: a primer*, 2nd edn. London: Academic Press.

Zhang J, Lu H, Liu M, Diao X, Shao K, Wu N. 2018. Phytolith analysis for differentiating between broomcorn millet (*Panicum miliaceum*) and its weed/feral type (*Panicum ruderale*). *Scientific Reports* **8**: 1–9.